Analyst

PAPER

View Article Online
View Journal | View Issue

Cite this: *Analyst*, 2022, **147**, 4049

Dual-strategy biosensing of glucose based on multifunctional $CuWO_4$ nanoparticles

Yu Zhang,*†[a] Shuang Li,†[a] Hongyuan Liu,[a] Feng Shi,[b] Juan Li,*[b] Xiaoya Hu[b] and Zhanjun Yang *[b]

Received 19th June 2022,
Accepted 22nd July 2022

DOI: 10.1039/d2an01003h

rsc.li/analyst

In this research, dual-strategy biosensing of glucose was proposed based on multifunctional $CuWO_4$ nanoparticles ($CuWO_4$ NPs), which were prepared for the application of electrochemical and colorimetric sensing of glucose. $CuWO_4$ NPs show large specific surface area and good conductivity as well as excellent peroxidase-like activity. A sensitive and selective electrochemical glucose biosensor was fabricated with the immobilization of glucose oxidase (GOx) on a $CuWO_4$ NP modified electrode for enhancing the direct electron transfer behavior. A wide linear range of 0.005–1.8 mM with a low detection limit of 1.5 μM and a high sensitivity of 28.02 mA M^{-1} cm^{-2} were achieved by using the electrochemical biosensor. Meanwhile, a colorimetric and visual glucose biosensor was constructed based on the GOx/$CuWO_4$ cascade nanozyme, which shows a linear range of 0.05–1.0 mM with excellent selectivity. $CuWO_4$ NPs as a promising matrix open up a dual-strategy biosensor for sensitive and selective detection of glucose.

Introduction

According to statistics, there are about 463 million diabetes patients worldwide, and this number is expected to increase to 578.4 million by 2030.[1] Long-term high glucose levels in the human body can cause many impairments, including microvascular disease, macrovascular disease, and peripheral neuropathy, all leading to deterioration of the quality of life of patients.[2–5] Therefore, detection of glucose levels is very important for people suffering from diabetes. In the past decades, varieties of methods have been investigated to detect glucose including fluorescence, optical and electrochemical detection.[6–9] Taking advantage of their high speed, high sensitivity, simple operation, and low cost, electrochemical biosensors have been widely utilized.[10–17] Also, colorimetric analysis has been developed for determination of glucose owing to its simple and easy operation.[18] Many kinds of nanomaterials have been widely utilized to load glucose oxidase (GOx) for fabricating sensitive electrochemical and colorimetric glucose biosensors.[19–21]

Tungstate materials have gained wide attention owing to excellent catalytic and electrochemical performances. $CuWO_4$ has high electrical conductivity, and it has a certain ability to absorb visible light and exhibits excellent stability under weak alkaline, neutral and acidic conditions.[22] The fabrication of $CuWO_4$ is mainly achieved from the combination of anions and cations to form a precipitate. The synthesis methods mainly include high temperature calcination,[23] a co-precipitation method,[24,25] a sol–gel method,[26] and an electrochemical deposition method.[27] $CuWO_4$ has been developed to use in a vast variety of fields, such as photo-electrolysis, photocatalysis, optical fibers, solar-assisted water splitting and sensors.[28–30] Since Yan's group revealed the peroxidase (POD)-like activity of Fe_3O_4 nanoparticles, more and more nanomaterials have been developed as nanozymes with intrinsic enzyme-like catalytic activity.[31–35] In light of the excellent POD-like activity of nanozymes, visual detection based on cascade nanozymes for biomolecules *via* colorimetric analysis has attracted more attention.[36,37] It is worth noting that $CuWO_4$ was investigated and found to possess high peroxidase-like activity.[38] To date, the applications of $CuWO_4$ materials have been mainly reported in the fields of photo-electrochemistry and photocatalysis,[39,40] but there are few studies on their use in electrochemical biosensors and colorimetric cascade nanozyme biosensing.

Herein, we synthesized $CuWO_4$ nanoparticles ($CuWO_4$ NPs) by a simple solvothermal route and they were exploited for the first time for the dual-strategy of electrochemical and colorimetric glucose biosensing (shown in Scheme 1). $CuWO_4$ NPs were utilized for modifying an electrode to immobilize enzymes and construct a novel electrochemical glucose

[a]*School of Nursing, Yangzhou University, Yangzhou 225000, PR China. E-mail: yizhangyu@yzu.edu.cn; Fax: +86-514-87978842; Tel: +86-514-87978842*
[b]*College of Chemistry and Chemical Engineering, Yangzhou University, Yangzhou 225002, PR China. E-mail: zjyang@yzu.edu.cn, lijuan@yzu.edu.cn; Fax: +86-514-87972034; Tel: +86-514-87972034*
†These authors contributed equally to this work.

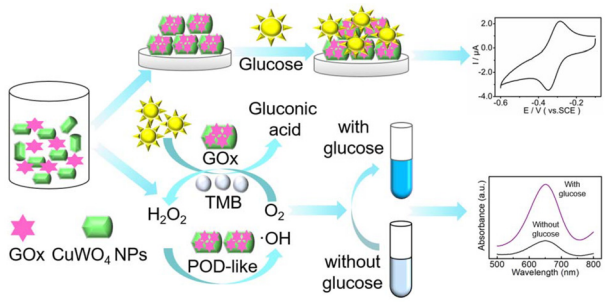

Scheme 1 The schematic of constructing electrochemical and colorimetric glucose biosensors.

biosensor. $CuWO_4$ nanostructures possess a larger surface area and give a well biocompatible substrate, which can facilitate direct electron transfer between the immobilized enzyme and the surface of the electrode. In addition, in light of the POD-like activity of $CuWO_4$ NPs, a GOx/$CuWO_4$ cascade nanozyme was prepared for detection of glucose. This can be ascribed to GOx being able to catalyze the oxidation of glucose to form H_2O_2 and gluconic acid; at the same time, $CuWO_4$ with peroxidase activity can catalyze H_2O_2 to form HO$^{\bullet}$ for catalyzing the oxidation of TMB to ox-TMB with an apparent blue color causing an obvious absorption peak. This work provides a potential multifunctional material for developing dual-mode glucose biosensors.

Materials, apparatus and methods

Materials and reagents

GOx (EC 1.1.3.4, 108 U mg^{-1}, from *Aspergillus niger*) was purchased from Ameresco. 1-(3-Dimethylaminopropyl)-3-ethylcarbodiimide hydrochloride (EDC), *N*-hydroxysuccinimide (NHS) and 11-mercaptoundecanoic acid (MUA) were purchased from Sigma-Aldrich. Nafion and D-(+)-glucose were supplied by Sigma-Aldrich. 3,3′,5,5′-Tetramethylbenzidine (TMB) was purchased from America Acros. $CuCl_2$, Na_2WO_4, ethanol and HCl were supplied by Sinopharm Chemical Reagent Co., Ltd. The prepared stock solution of D-glucose was stored for a whole day at room temperature prior to use. To prepare phosphate buffer solution (PBS), 0.1 M NaH_2PO_4 and Na_2HPO_4 were mixed; afterwards, H_3PO_4 or NaOH solution was used to adjust the pH of the PBS. All other reagents and chemicals were of analytical grade; furthermore, the corresponding solutions were prepared utilizing distilled water.

Apparatus

A CHI 660e electrochemical workstation (Co., CHI, Shanghai Chenhua, China) was applied to complete electrochemical experiments. A three-electrode system was utilized in all experiments, in which a saturated calomel electrode (SCE) as the reference electrode, a glassy carbon electrode (GCE, D = 3 mm) as the working electrode and platinum wire as the auxiliary electrode were used. Cyclic voltammetry experiments were performed in an electrochemical cell implanted with 10.0 mL of buffer solution at a scanning rate of 100 mV s^{-1}. All pH values were measured *via* an S-25 digital pH-meter and a glass composite electrode. The transmission electron micrographs (TEM) were acquired with a Philips Tecnai 12 microscope (Holland) at 120 kV accelerating voltage. A Hitachi S-4800 scanning electron microscope (Japan) was used to obtain the scanning electron micrographs (SEM) at 15 kV accelerating voltage. A D8 advanced X-ray diffractometer (Bruker Co., Germany) was used for investigating X-ray diffraction (XRD) patterns at room temperature. Ultraviolet–visible (UV-vis) experiments were completed with a UV2500 spectrophotometer (Beijing General Instrument Co., Ltd).

Methods of synthesizing $CuWO_4$ nanoparticles

The $CuWO_4$ NPs were synthesized *via* a simple solvothermal method by our group. In a typical procedure, 10 mM $CuCl_2$ and 10 mM Na_2WO_4 were dissolved separately in 25 mL of distilled water under ultrasonication for 5 minutes, and then the Na_2WO_4 solution was added to the $CuCl_2$ solution drop by drop. The mixture was sonicated for 1.0 h and heated to 90 °C until it was dried. After that, the mixture was heated to 350 °C and this temperature was maintained for 3 hours under air. Finally, the obtained powder was washed using ethanol and water, in sequence, and dried overnight at 60 °C.

Preparation of a $CuWO_4$ NP-based electrochemical glucose biosensor

1.0 mg of $CuWO_4$ NPs was dissolved in 1.0 mL of distilled water by ultrasonicating for 10 minutes. Then, 1.0 mg of GOx was added into 100 μL of the above suspension and the mixture was shaken evenly. 10.0 μL of the mixture was coated on the surface of the prepared GCE and placed in a refrigerator to dry. After coating 10.0 μL of 0.5% Nafion on GOx/$CuWO_4$ NPs/GCE to form a membrane and prevent the mixture from falling off, the final electrodes were obtained. Distilled water was used to clean the obtained electrodes thoroughly to remove those GOx molecules that were loosely adsorbed. The enzyme electrodes were placed in a refrigerator at a low temperature of 4 °C before subsequent measurements.

The preparation of the GOx/$CuWO_4$ cascade nanozyme sensor

The GOx/$CuWO_4$ cascade nanozyme sensor was prepared for the colorimetric visual detection of glucose. 4 mg of $CuWO_4$ NPs was dispersed in phosphate buffer solution (pH 7.4) *via* ultrasonication and then 400 μL of MUA was added into the dispersion for the carboxylation of $CuWO_4$ while stirring. After stirring for 2 h, 200 μL of EDC and 140 μL of NHS were injected into the mixture for activating carboxyl and stirring was maintained for 1 h. Then, to complete the formation of the GOx/$CuWO_4$ cascade nanozyme, 4 mg of GOx was added and mixed *via* stirring under an ice bath for 3 h. Eventually, the mixture was centrifuged and redispersed in 4 mL of PBS. The obtained GOx/$CuWO_4$ cascade nanozyme was stored at 4 °C before use.

The assessment of peroxidase-like catalytic activity

It is well known that 3,3′,5,5′-tetramethylbenzidine (TMB) can be oxidized showing an intense blue color under the coexistence of H_2O_2 and peroxidase, which can be attributed to the oxidative hydroxyl radical from H_2O_2 catalysed by the peroxidase. Thus, the colorimetric assay, which was achieved *via* the catalytic oxidation of the substrate 3,3′,5,5′-tetramethylbenzidine (TMB) with the existence of hydrogen peroxide (H_2O_2), was utilized to study the intrinsic peroxidase activity of the $CuWO_4$ NPs. The influence of the pH of acetate buffer solution (ABS) on the peroxidase-like activity of $CuWO_4$ was investigated *via* changing the pH of the acetate buffer. All the colorimetric experiments were performed in 0.2 M acetate buffer and the absorbance at 652 nm was detected using a UV-vis spectrophotometer. For POD-like activity detection and the determination of glucose, 100 μL of 1 mg mL^{-1} $CuWO_4$, 20 μL of 30% H_2O_2, and 50 μL of 20 mg mL^{-1} TMB were added, and the total volume was maintained at 2 mL.

Colorimetric determination of glucose

The glucose was determined by colorimetric analysis *via* a UV-vis spectrophotometer according to the mechanism that GOx can catalyse the oxidation of glucose to form H_2O_2 and gluconic acid; at the same time, $CuWO_4$ with peroxidase activity can catalyse H_2O_2 to form $HO^{\bullet}$ for catalysing the oxidation of TMB to ox-TMB with an apparent blue color causing an obvious absorption peak. For glucose detection, to a reaction volume of 2 mL, 100 μL of GOx/$CuWO_4$, 50 μL of 20 mg mL^{-1} TMB and different volumes of 0.01 M glucose and acetate buffer (pH 4.5) were mixed and the resulting mixture was incubated in a 5 ml centrifuge tube for 30 min. After that, the mixture was transferred into a cuvette and measured on a UV-vis spectrophotometer for detecting the glucose with the observed absorbance at 652 nm.

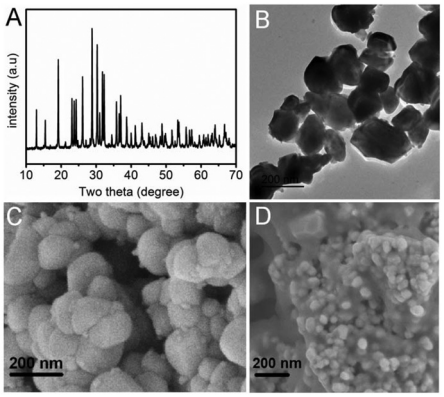

Fig. 1 XRD spectra (A), and TEM (B) and SEM (C) images of the $CuWO_4$ NPs, and (D) the SEM image of GOx/$CuWO_4$ NPs.

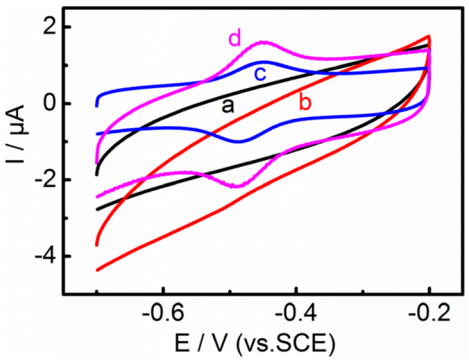

Fig. 2 Cyclic voltammograms of Nafion/GCE (a), $CuWO_4$ NPs/Nafion/GCE (b), Nafion/GOx/GCE (c) and GOx/$CuWO_4$ NPs/Nafion/GCE (d) in N_2-saturated 0.1 M pH 7.0 PBS at 100 mV s^{-1}.

Results and discussion

Study on the electrochemical detection of glucose

Characterization of the $CuWO_4$ NPs and enzyme electrode. The structure and morphology of $CuWO_4$ NPs were investigated using several characterization studies. Fig. 1A illustrates the typical XRD pattern of the fabricated $CuWO_4$ NPs. The single hexagonal phase of $CuWO_4$ can be exactly indexed by all diffraction peaks (JCPDS card no. #21-0307), demonstrating the successful fabrication of $CuWO_4$ NPs. Fig. 1B and C exhibit the SEM and TEM images of $CuWO_4$ NPs, which show that $CuWO_4$ is composed of irregular particles with a uniform size of 100 nm. This special nanostructure exhibits a large specific surface area to trap more enzyme molecules. After the immobilization of GOx on the $CuWO_4$ NPs, a SEM image presents the different morphology of GOx/$CuWO_4$ NPs (Fig. 1D) in comparison with a single $CuWO_4$ NP, implying that GOx was favourably loaded on the surface of $CuWO_4$ NPs.

Direct electrochemical behavior at GOx/$CuWO_4$ NPs/Nafion/GCE. Fig. 2 indicates the cyclic voltammograms of various types of modified glassy carbon electrodes in 0.1 M nitrogen-saturated phosphate buffer solution at a scan rate of 100 mV s^{-1}. There were no peaks in the CVs at Nafion/GCE (curve a) and $CuWO_4$ NPs/Nafion/GCE (curve b). As expected, GOx/Nafion/GCE (curve c) shows a couple of well-defined and weak oxidation and reduction peaks, but GOx/$CuWO_4$ NPs/Nafion/GCE shows a pair of better-defined and intense oxidation and reduction peaks (curve d) at −0.452 and −0.491 V, demonstrating that the $CuWO_4$ NPs promote direct electron transfer between the surface of the electrode and GOx effectively. The reduction peak current of GOx/Nafion/GCE is only one quarter of that of GOx/$CuWO_4$ NPs/Nafion/GCE, which is attributed to the unique structure and high electrical conductivity of $CuWO_4$ NPs.

Detection mechanism and capability of the electrochemical glucose biosensor. The cyclic voltammograms of $CuWO_4$ NPs/Nafion/GCE and GOx/$CuWO_4$ NPs/Nafion/GCE are depicted in Fig. 3. The electrochemical experiments were carried out in a N_2 and air-saturated pH 7.0 phosphate buffer solution in the presence or absence of glucose. In the nitrogen-saturated PBS, there was no obvious redox peak in the cyclic voltammogram of $CuWO_4$ NPs/Nafion/GCE (curve a of Fig. 3A). In the air-saturated phosphate buffer solution, a slight increase of the reduction peak current was shown in the cyclic voltammogram

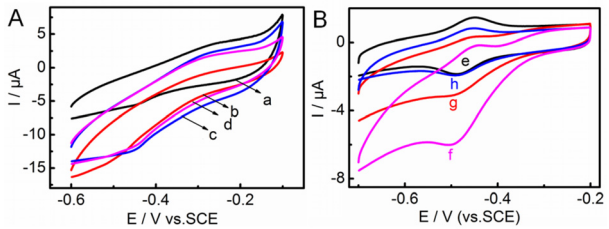

Fig. 3 (A) Cyclic voltammograms of $CuWO_4$ NPs/Nafion/GCE in N_2-saturated PBS (0.1 M, pH 7.0) (a), air-saturated PBS (b), and air-saturated PBS including 0.5 (c) and 1.0 mM (d) glucose at 100 mV s^{-1}; (B) cyclic voltammograms of GOx/$CuWO_4$ NPs/Nafion/GCE in 0.1 M pH 7.0 nitrogen-saturated PBS (e), air-saturated PBS (f) and air-saturated PBS including 0.5 (g) and 1.0 mM (h) glucose.

of $CuWO_4$ NPs/Nafion/GCE (curve b in Fig. 3A). Afterwards, on adding glucose into the air-saturated electrolyte, there was no apparent increase of the reduction peak current of $CuWO_4$ NPs/Nafion/GCE (curves c and d of Fig. 3A). However, GOx/$CuWO_4$ NPs/Nafion/GCE shows an obvious redox peak in the nitrogen-saturated solution (curve e of Fig. 3B). Similarly, in the air-saturated solution the reduction peak current became vividly stronger (curve f in Fig. 3B). It can be seen from formulas (1) and (2) that the results suggest that a representative dissolved oxygen electrocatalytic process is performed in GOx/$CuWO_4$ NPs/Nafion/GCE. On increasing the content of glucose, the reduction peak current clearly decreased at GOx/$CuWO_4$ NPs/Nafion/GCE (curves g and h). According to formula (3), the result may be related to the inhibition of the electrocatalytic reaction by the reaction catalysed by enzyme molecules at GOx/$CuWO_4$ NPs/Nafion/GCE. On the basis of the current change at GOx/$CuWO_4$ NPs/Nafion/GCE in response to glucose, an electrochemical enzymatic biosensor was constructed for monitoring the level of glucose quantitatively.

$$\mathrm{GOx\ (FAD)}\ 2e^- + 2H^+ \leftrightarrow \mathrm{GOD\ (FADH_2)} \quad (1)$$

$$\mathrm{GOx\ (FADH_2)} + O_2 \rightarrow \mathrm{GOD\ (FAD)} + H_2O_2 \quad (2)$$

$$\mathrm{Glucose + GOx(FAD) + O_2 \rightarrow gluconolactone + GOx(FADH_2)} \quad (3)$$

Performance of the electrochemical glucose biosensor. Fig. 4A exhibits the cyclic voltammograms of GOx/$CuWO_4$ NPs/Nafion/GCE obtained in air-saturated phosphate buffer solution at pH 7.0 with the continuous addition of glucose. In the range of 0.005 to 1.8 mM, the current responses of GOx/$CuWO_4$ NPs/Nafion/GCE were enhanced linearly with increasing glucose content (Fig. 4B). The sensitivity and the detection limit were calculated to be 28.02 mA M^{-1} cm^{-2} and 1.5 μM, respectively, which are better than those of other semiconductor nanomaterial-based electrochemical glucose sensors.[41–43]

Fig. 4C presents the trace following addition of interferents during the quantitative detection of glucose. The amperometric response increased apparently after adding 0.1 mM glucose into the pH 7.0 buffer solution. Conversely, there was almost no obvious current response change when adding 0.1 mM ascorbic acid (AA), acetamidophenol (AP) and uric acid (UA) into the electrolyte solution in sequence. However, the current increased obviously after again adding 0.1 mM glucose. The obtained results indicate that the biosensor possesses exceptional selectivity and anti-interference ability.

Study on the colorimetric analysis of glucose based on the GOx/$CuWO_4$ cascade nanozyme

Investigation of POD-like activity of $CuWO_4$ NPs. The intrinsic POD-like activity of $CuWO_4$ NPs was studied *via* classical colorimetry. As apparently depicted in Fig. 5A, an obvious absorption peak occurs at 652 nm in the presence of $CuWO_4$ NPs, H_2O_2 and TMB under an ABS acidic environment (0.2 M, pH 4.5). This is because the peroxidase-like activity of $CuWO_4$ NPs allows catalysis of hydrogen peroxide to generate reactive oxygen free radicals in the presence of hydrogen peroxide, which can oxidize TMB to form TMBox with a strong blue color (inset d). However, there is no clear absorption peak in the absence of hydrogen peroxide and the mixture containing $CuWO_4$, TMB, and their corresponding solutions, shows no obvious colour (insets a–c). The above experimental results prove that $CuWO_4$ possesses good peroxidase-like activity.

In addition, Fig. 5B shows the effect of acetate buffer pH ranging from 2.5–9.5 on the peroxidase-like activity of the $CuWO_4$ NPs. It can be seen from Fig. 5B that the activity of $CuWO_4$ NPs reaches a maximum value at pH 4.5, which is ascribed to the easy formation of $HO^{\bullet}$ in a weakly acidic medium. The conversion of H_2O_2 in a strongly acidic medium

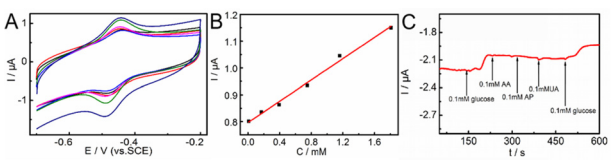

Fig. 4 (A) Cyclic voltammograms showing GOx/$CuWO_4$ NPs/Nafion/GCE in pH 7.0 air-saturated PBS responding to continuous addition of different concentrations of glucose; (B) calibration curve of GOx/$CuWO_4$ NPs/Nafion/GCE for glucose; (C) amperometric response of GOx/$CuWO_4$ NPs/Nafion/GCE in 0.1 mM glucose, AA, UA, and AP in pH 7.0 PBS.

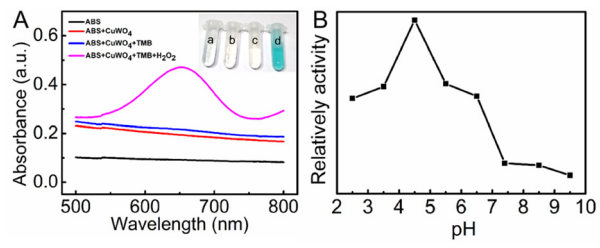

Fig. 5 (A) Study on the POD-like activity of the $CuWO_4$ NPs in ABS (inset a), ABS + $CuWO_4$ (inset b), ABS + $CuWO_4$ + TMB (inset c), and ABS + $CuWO_4$ + TMB + H_2O_2 (inset d) at 652 nm; (B) the influence of pH values ranging from 2.5 to 9.5 on the POD-like activity of $CuWO_4$ NPs.

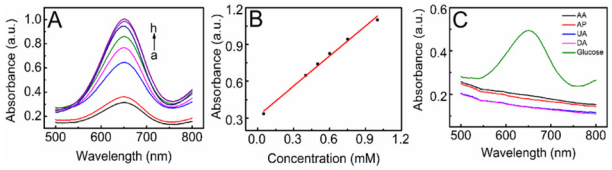

Fig. 6 (A) Absorbance of the continuous addition of different concentration of glucose based on the GOx/$CuWO_4$ NP cascade nanozyme in ABS (0.2 M, pH 4.5); (B) calibration curve of the colorimetric analysis for glucose; (C) absorbance of 0.01 M of glucose, 0.01 M of AA, 0.01 M of AP, 0.01 M of UA and 0.01 M of DA in ABS (0.2 M, pH 4.5).

leads to a decrease of $HO^{\bullet}$, demonstrating low peroxidase-like activity. Nevertheless, $HO^{\bullet}$ will react with H_2O_2 to form $O_2^{\bullet-}$ with weak oxidizing ability, and $OH^{\bullet}$ can react with $O_2^{\bullet-}$ to form OH^- and O_2, so that the $OH^{\bullet}$ content decrease suggests a decrease of peroxidase-like activity. Therefore, the pH of the ABS was selected as 4.5.

Colorimetric detection of glucose

A glucose colorimetric sensor based on the GOx/$CuWO_4$ cascade nanozyme was constructed to quantitatively detect glucose content using a UV-vis spectrophotometer. As shown in Fig. 6A, the UV-vis absorbance value at 652 nm increased gradually with the elevation of glucose concentration. In addition, as described in Fig. 6B, the colorimetric sensor constructed based on the cascade enzyme possesses a linear range of 0.05–1.0 mM for glucose detection with a linear correlation coefficient of 0.9927. The detection limit of 0.016 mM is lower than that of colorimetric biosensors for glucose based on other nanozymes.[44,45] The experimental results prove that the constructed colorimetric biosensor can be applied to monitor glucose visually.

Considering the interference of other biomolecules in practical detection, 0.01 M ascorbic acid (AA), acetamidophenol (AP), uric acid (UA) and dopamine hydrochloride (DA) were selected as interferents added into the detection system. It can be seen from Fig. 6C that the absorbance was elevated significantly in the presence of glucose, while there was no obvious absorption peak in the presence of AA, AP, UA, and DA. These results demonstrated that the constructed colorimetric biosensor based on the GOx/$CuWO_4$ cascade enzyme provides excellent selectivity for the determination of glucose.

Conclusions

Multifunctional $CuWO_4$ nanoparticles were prepared for application in the dual-strategy biosensing of glucose. A sensitive electrochemical glucose biosensor was fabricated *via* immobilizing glucose oxidase (GOx) on the $CuWO_4$ NPs for enhancing the properties of the biosensor, which is attributed to the large specific surface area and good conductivity of the $CuWO_4$ NPs. Moreover, a colorimetric analysis based on the GOx/$CuWO_4$ NP cascade enzyme was proposed to detect glucose due to the good peroxidase-like activity of $CuWO_4$ NPs. The proposed electrochemical and colorimetric biosensor exhibited good sensitivity and excellent selectivity. This work develops dual-strategy biosensing of glucose, which provides a new choice for constructing a biosensor for detection of biomolecules.

Conflicts of interest

The authors declare no competing interests.

Acknowledgements

The authors acknowledge the financial support from the National Natural Science Foundation of China (21575125, 21475116), the Natural Science Foundation of Jiangsu Province (BK20221370, BK20191434), the Priority Academic Program Development of Jiangsu Higher Education Institution (PAPD), the Project for Science and Technology of Yangzhou (YZ2020068), and the Postgraduate Research & Practice Innovation Program of Jiangsu Province (no. KYCX17_1876).

References

1 P. Saeedi, I. Petersohn, P. Salpea, B. Malanda, S. Karuranga, N. Unwin, S. Colagiuri, L. Guariguata, A. A. Motala, K. Ogurtsova, J. E. Shaw, D. Bright and R. Williams, *Diabetes Res. Clin. Pract.*, 2019, **157**, 107843.
2 R. B. Brown, *Curr. Diabetes Rev.*, 2020, **16**(7), 674–689.
3 H. Karami, M. S. Shiri, A. Rezapour, R. S. Mehrabadi and S. Afshari, *Qual. Life Res.*, 2021, **30**(7), 1963–1974.
4 Q. X. Gan, J. Wang, J. Hu, G. H. Lou, X. J. Xiong, C. Y. Peng, S. Zheng and Q. W. Huang, *J. Steroid Biochem.*, 2020, **198**, 105575.
5 T. B. Pham, T. T. Nguyen, H. T. Truong, C. H. Trinh, H. N. T. Du, T. T. Ngo and L. H. Nguyen, *J. Diabetes Res.*, 2020, **2020**, 4360804.
6 I. L. Jernelv, K. Milenko, S. S. Fuglerud, D. R. Hjelme, R. Ellingsen and A. Aksnes, *Appl. Spectrosc. Rev.*, 2019, **54**, 543–572.
7 E. Sehit and Z. Altintas, *Biosens. Bioelectron.*, 2020, **159**, 112165.
8 S. A. Zaidi and J. H. Shin, *Talanta*, 2016, **149**, 34–42.
9 N. S. Oliver, C. Toumazou, A. E. G. Cass and D. G. Johnston, *Diabetic Med.*, 2009, **26**, 197–210.
10 J. Li, Y. T. Liu, X. Tang, L. J. Xu, L. F. Min, Y. D. Xue, X. Y. Hu and Z. J. Yang, *Microchim. Acta*, 2020, **187**(1), 80.
11 C. Zhou, Y. Shi, X. Ding, M. Li, J. Luo, Z. Lu and D. Xiao, *Anal. Chem.*, 2013, **85**(2), 1171–1176.
12 F. Shi, J. Y. Li, J. X. Xiao, X. X. Ma, Y. D. Xue, J. Li, M. Shen and Z. J. Yang, *Analyst*, 2022, **147**, 430–435.
13 Y. C. Yan, Z. J. Qiao, X. Hai, W. L. Song and S. Bi, *Biosens. Bioelectron.*, 2021, **174**, 112827.

14 F. Shi, J. M. Xu, Z. F. Hu, C. L. Ren, Y. D. Xue, Y. C. Zhang, J. Li, C. Y. Wang and Z. J. Yang, *Chin. Chem. Lett.*, 2021, **32**(10), 3185–3188.
15 X. Xu, S. Jiang, Z. Hu and S. Liu, *ACS Nano*, 2010, **4**(7), 4292–4298.
16 J. Li, T. Yan, J. Yang, Z. J. Yang, Y. C. Zhang and X. Y. Hu, *Sens. Actuators, B*, 2014, **190**, 549–554.
17 Y. L. Wu, Q. W. Li, X. L. Zhang, X. Chen and X. M. Wang, *Chin. Chem. Lett.*, 2013, **12**, 1087–1090.
18 X. C. Li, C. B. Li, S. D. Zhang, C. J. Cui, J. X. Li and Q. Q. Gao, *Anal. Bioanal. Chem.*, 2021, **413**, 5725–5731.
19 Z. J. Yang, Y. B. Xu, J. Li, Z. Q. Jian, S. H. Yu, Y. C. Zhang, X. Y. Hu and D. D. Dionysiou, *Microchim. Acta*, 2015, **182**, 1841–1848.
20 S. Y. Dong, N. Li, G. C. Suo and T. L. Huang, *Anal. Chem.*, 2013, **85**, 11739.
21 J. Li, M. M. Lu, Z. N. Tan, Y. B. Xu, Y. C. Zhang, X. Y. Hu and Z. J. Yang, *Microchim. Acta*, 2016, **183**, 1705–1712.
22 O. Y. Khyzhun, V. L. Bekenev and Y. M. Solonin, *J. Alloys Compd.*, 2009, **480**(2), 184–189.
23 L. P. Dorfman, D. L. Houck, M. J. Scheithauer, J. N. Dann and H. O. Fa Ssett, *J. Mater. Res.*, 2001, **16**(4), 1096–1102.
24 T. Montini, V. Gombac, A. Hameed, L. Felisari, G. Adami and P. Fornasiero, *Chem. Phys. Lett.*, 2010, **498**(1), 113–119.
25 A. E. B. Lima, M. J. S. Costa, R. S. Santos, N. C. Batista, L. S. Cavalcante, E. Longo and G. E. Luz, *Electrochim. Acta*, 2017, **256**, 139–145.
26 K. J. Pyper, J. E. Yourey and B. M. Bartlett, *J. Phys. Chem. C*, 2013, **117**(47), 24726.
27 J. E. Yourey and B. M. Bartlett, *J. Mater. Chem.*, 2011, **21**, 21.
28 U. M. García-Pérez, A. M. Cruz and J. Peral, *Electrochim. Acta*, 2012, **81**, 227–232.
29 G. Hitoki, T. Takata, S. G. Ikeda, M. Hara, J. N. Kondo, M. Kakihana and K. Domen, *Catal. Today*, 2000, **63**(2), 175–181.
30 J. E. Yourey, K. J. Pyper, J. B. Kurtz and B. M. Bartlett, *J. Phys. Chem. C*, 2013, **117**(17), 8708–8718.
31 A. Karthika, P. Karuppasamy, S. Selvarajan, S. Suganthi and M. Rajarajan, *Ultrason. Sonochem.*, 2019, **55**, 196–206.
32 L. Jiao, W. Q. Xu, Y. Zhang, Y. Wu, W. L. Gu, X. X. Ge, B. B. Chen, C. Z. Zhu and S. J. Guo, *Nano Today*, 2020, **35**, 100971.
33 X. Y. Zhou, F. Chun, Q. W. Tian, C. H. Han, Z. Q. Yin, Z. Y. Dong and S. Bi, *Anal. Chem.*, 2022, **94**(2), 847–855.
34 H. Zhang, W. K. Kang, Y. Wang, X. Z. Wang and L. H. Lu, *J. Anal. Test.*, 2022, **6**, 3–11.
35 X. Hai, X. Y. Zhu, K. X. Yu, S. Z. Yue, W. L. Song and S. Bi, *Biosens. Bioelectron.*, 2021, **192**, 113544.
36 X. X. Li, Q. W. Huang, W. Li, J. L. Zhang and Y. Fu, *J. Anal. Test.*, 2019, **3**, 277–285.
37 K. Aneesh, C. S. Raovusa and S. Berchmans, *Sens. Actuators, B*, 2017, **253**, 723–730.
38 W. Ye, F. Chen, F. Zhao, N. Han and Y. Li, *ACS Appl. Mater. Interfaces*, 2016, **8**(14), 9211–9217.
39 C. R. Lhermitte and B. M. Bartlett, *Acc. Chem. Res.*, 2016, **49**(6), 1121–1129.
40 T. Mavrič, M. Valant, M. Forster, A. J. Cowan, U. Lavrenčič and S. Emin, *J. Colloid Interface Sci.*, 2016, **483**, 93–101.
41 X. F. Hoo, K. A. Razak, N. S. Ridhuan, N. M. Nor and N. D. Zakaria, *J. Mater. Sci.: Mater. Electron.*, 2019, **30**, 7460–7470.
42 L. Wang, J. Li, M. J. Feng, L. F. Min, J. Yang, S. H. Yu, Y. C. Zhang, X. Y. Hu and Z. J. Yang, *Biosens. Bioelectron.*, 2017, **96**, 220–226.
43 W. Tang, L. Li and X. Zeng, *Talanta*, 2015, **131**, 417–423.
44 X. M. Wu, J. T. Yin, J. F. Liu, Y. Gu, S. Wang and J. P. Wang, *Analyst*, 2020, **145**, 7234–7241.
45 H. T. Chen, C. Y. Yuan, X. Y. Yang, X. W. Cheng, A. A. Elzatahry, A. Alghamdi, J. C. Su, X. He and Y. H. Deng, *ACS Appl. Nano Mater.*, 2020, **3**(5), 4586–4598.